Arch. Metall. Mater. **68** (2023), 2, 463-468

DOI: https://doi.org/10.24425/amm.2023.142423

A. SAPIETOVÁ[1*], M. RAČEK[1], V. DEKÝŠ[1], M. SAPIETA[1], M. SÁGA[1], P. ŠOFER[2]

ACOUSTIC EMISSION AND INFRARED THERMOGRAPHY STUDY OF LOW STRAIN TENSILE BEHAVIOUR OF AISI 304L STAINLESS STEEL

In-situ study of deformation behaviour and mechanisms occurring during early stages of deformation is of a great practical importance. Low stacking fault energy materials, as is the case of AISI 304L, show non-linear deformation characteristics way below the bulk yield point. Shockley partial dislocations, formation of stacking faults respectively, resulting in creation of shear bands and ε-martensite transformation are the mechanisms occurring in the low strains in the studied steel. Acoustic emission and infrared thermography have been used in this study to investigate the deformation kinetics at the low strain stages of slow strain rate tensile tests. Acoustic emission cumulative energy together with the tracking of specimen maximum temperature have been found to be very useful in-situ techniques both supplementing each other in the sense of the sensitivity to different mechanisms. Mechanical, acoustic emission and infrared thermography results are discussed in detail with respect to potential occurred mechanism.

Keywords: Acoustic Emission; Infrared Thermography; Stainless Steel; Tensile Deformation

1. Introduction

AISI 304/304L is the widely used stainless steel (SS) grade which application range spans from the simple constructions like the handrails to the cryogenic pressure vessels used in chemical industry. Non-deformed crystal structure of annealed AISI 304/304L SS consists of austenite-γ with face-centred cubic (FCC) unit cells [1]. On plastic deformation of FCC low stacking fault energy (SFE) metals the perfect dislocations dissociate to Shockley partial dislocations and the stacking faults (SF) are taking place. With progressing straining, SFs overlapp on austenite $\{1\ 1\ 1\}_\gamma$ planes and form the shear bands. SFs overlapped on every second $\{1\ 1\ 1\}_\gamma$ plane create the hexagonal close-packed (HCP) structure of ε-martensite, whereas the overlapping on successive $\{1\ 1\ 1\}_\gamma$ planes generates mechanical twins [2,3]. From moderate to high strains, α'-martensite transforms either directly from austenite γ or from ε-martensite [4,5]. There are many papers investigating the microstructure of tensile deformation of AISI 304, whether post-mortem after the specific stages of deformation [4-6] or in situ [7,8]. Despite the number of experiments the results are not consistent mainly in terms of strains where the specific mechanisms occur. This is expectable regarding the strong sensitivity of deformation behaviour to variation on SFE, loading rate, and temperature respectively. Within the AISI 304 SS grade the relatively large span of essential stabilizing component as Ni, Cr, C affects the material SFE significantly. Dependence of mechanisms on SFE obtained by Sato et al. [2] for Fe-Mn-Al austenitic alloys shows the occurrence of ε-martensite under 20 mJm^{-2} and twinning above this SFE value. Allain et al [3] have reported the occurrence of ε-martensite under 18 mJm^{-2} and twinning in the range 12-35 mJm^{-2} for Fe-Mn-C austenitic alloys. Furthermore Galindo-Nava et al [4] have shown the area of coexistence of ε-martensite, α'-martensite and twinning in the range of 13-22 mJm^{-2} at 20% strain, stated through the wide scale of austenitic steel grades. Distinguishing between mechanisms in low deformation stages is a challenging task but with a great practical importance as most of the devices are designed to operate in assumed elastic stage with respect to bulk yield point. Non-destructive in-situ tools enabling to capture the changes in mechanisms is thus very desirable. Acoustic emission (AE) and infrared thermography (IRT) are relevant techniques detecting the portion of dissipated energy directly connected to the occurred process. In this paper AE and IRT have been used to distinguish the changes in mechanisms below 7% strain.

[1] UNIVERSITY OF ŽILINA, FACULTY OF MECHANICAL ENGINEERING, DEPARTMENT OF APPLIED MECHANICS, UNIVERZITNÁ 8215/1, 010 26 ŽILINA, SLOVAK REPUBLIC
[2] VŠB-TECHNICAL UNIVERSITY OF OSTRAVA, FACULTY OF MECHANICAL ENGINEERING, DEPARTMENT OF CONTROL SYSTEMS AND INSTRUMENTATION, 17. LISTOPADU 15/2127, 708 33 OSTRAVA-PORUBA, CZECH REPUBLIC

* Corresponding author: alzbeta.sapietova@fstroj.uniza.sk

2. Experimental

A set of eight slow strain rate tensile experiments has been conducted using Testometric M500-50CT, 25 kN tensile device. Dog bone specimens with the gauge cross section 3×10 mm and gauge length 70 mm were milled from the commercial hot rolled and annealed bars of AISI 304L SS. The chemical composition of experimental steel is stated in the CHEMICAL COMPOSITION OF THE INVESTIGATED AISI 304 L SS IN (WT.%, FE BALANCE)1.

TABLE 1

Chemical composition of the investigated AISI 304 L SS in (wt.%, Fe balance)

C	Si	Mn	P	S	Cr	Ni	Co	N
0.024	0.41	1.49	0.034	0.003	18.05	8.03	0.245	0.069

Material SFE computed according to Schramm and Reed formula [5] (assigned as SFE_{S-R}) and Brofman and Ansell relation [6] (reffered as SFE_{B-A}) is as follows: $SFE_{S-R} = 14.2\ mJm^{-2}$, $SFE_{B-A} = 17.9\ mJm^{-2}$. Specimens were strained at room temperature by two rates: $\dot{\varepsilon} = 7\times10^{-4}\ s^{-1}$ and $\dot{\varepsilon} = 1.4\times10^{-4}\ s^{-1}$. The strain rates have been chosen to lie above and under $\dot{\varepsilon} = 5\times10^{-4}\ s^{-1}$, which is the value published by Li et al. [7] as the rate where the heat dissipation approaches the heat generation by adiabatic heating on plastic deformation and martensitic transformation in AISI 304 SS. Deformation has been measured using contact extensometer.

For AE measurements the state-of-the-art setup consisting of Vallen AMSY-6A system and Vallen AEP5 preamplifiers with 35dB gain has been used which meets the highest requirements of the practical applicability, e.g. the tests of high-pressure steel vessels [8]. AE waves have been captured using two wide-band Vallen VS45 and VS900 transducers with different sensitivity characteristics. Sensors have been placed on the shoulder part of the specimen at the same position and on opposite surfaces and clamped by rubber bands. Vallen acoustic grease has been used as a couplant ensuring the good transfer of elastic waves from sample surface to ceramic plate of the sensor. Two additional sensors (Vallen VS 900) have been placed on the upper and lower clamp of tensile device via magnetic holders serving as the guards. Signals with the first arrival on one of the guard sensors have been attributed to the noise and discarded from evaluated dataset. Data postprocessing has been done in Matlab software.

Several authors have addressed the use of a thermal imager to detect changes in the temperature of test specimens in mechanical tests [15,16]. The FLIR SC7200 camera (MWIR, InSb, 320×256 pixels) was used to detect the infrared radiation of the samples during the tensile tests. Native frame rates of 383 Hz and 100 Hz, respectively, were used in the measurements. An important parameter in quantitative temperature measurements with infrared detectors is the knowledge of the emissivity of the tested samples [17,18]. ThermaSpray 800 (emissivity 0.97) was applied to the test specimens before measurement. The frame rates of 383 Hz and 100 Hz, respectively, were used in the measurements. Data were processed in FLIR ResearchIR MAX and Diadem software (National Instruments), respectively. The camera with a cooled detector was used due to the possibility of using short integration times, to detect possible areas of the sample with increased radiation.

3. Results and discussion

Most of the energy released on the dislocation movement is dissipated as a heat in the crystal lattice, where the thermal energy can be considered as some sort of cumulative quantity. The increments of elastic strain, as the consequence of overcoming the energy barriers separating the positions of atoms, are being suddenly irreversibly released in the form of AE waves [9]. Thermal emission detected by medium wavelength infrared camera is represented by the maximum temperature tracked on the surface of specimen gauge. AE hit energy on the other hand is the other adequate parameter directly connected to the kinetics of plastic deformation mechanisms. Instead of analysing the AE energy of separated hits, it is more natural to visualize the cumulative energy of hits to unify the outputs of both NDE techniques. As a result, stress-strain curves together with the cumulative AE energy and maximum temperature has been visualized together to study the plastic deformation evolution in the low deformation stages. Strains up to 7% are analysed in this work. Accounting the computed SFE of investigated material the coexistence of γ, ε and α' phases and twinning could be expected [4]. Mechanical twins and transition of α′ martensite is assumed to occur at moderate and high strains [4,5,20,21]. Assumed mechanisms below 7% strain are thus Shockley partial dislocations and SF, shear bands, and ε-martensite transition. Shear bands must not be only ε-martensite bands and twinn bands but also the bands with faulted ε and faulted twinn as a result of irregular overlapping of SF in close-packed planes [10]

Typical mechanical data together with AE and IRT results for the sample strained at the rate $\dot{\varepsilon} = 7\times10^{-4}\ s^{-1}$ are plotted on Fig. 1. Stress strain curve for strain rate ε· = 7×10–4 s–1. Stress strain curve (red line) plotted with maximum temperature (black line) and AE cumulative energy (blue solid line – sensor VS900, blue dashed line – sensor VS45). Vertical dashed lines separate the stages I, II, and III1.

Behind the very short linear region (below 140 MPa) the stress-strain curve starts to show non-linear behaviour, which is the point of AE cumulative energy onset on both channels. Detectable AE waves are thus generated with the macroscopic stress changes, as it has been published by Zreihan et al. [11]. It is interesting to point out that even though the two AE sensors have different frequency sensitivity and some small variations in cumulative energy are prominent, both sensors reflect the same increasing trend with the non-linear stress-strain character below the assumed yield point. Small variations are probably caused by higher sensitivity of VS900 to the frequencies above approx. 450 kHz but lower sensitivity to the events below 200 kHz. Dur-

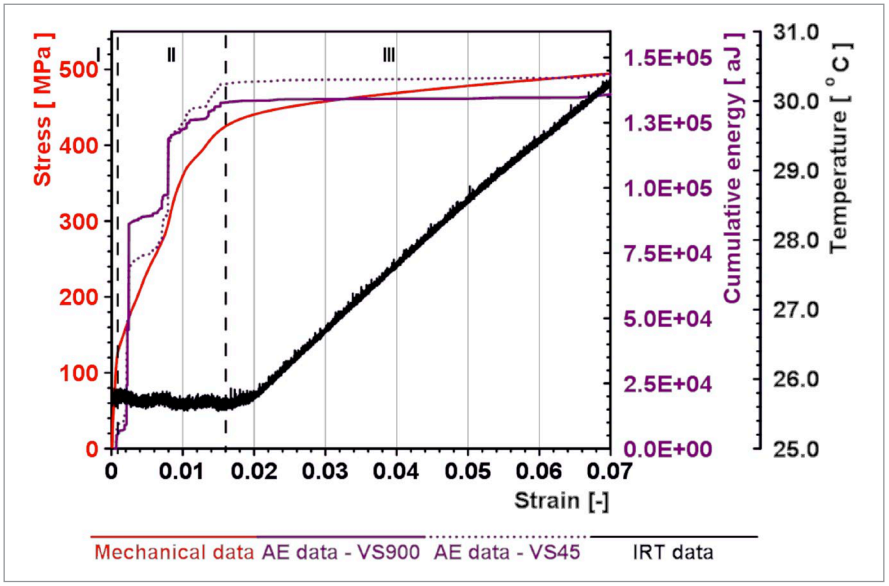

Fig. 1. Stress strain curve for strain rate $\dot{\varepsilon} = 7\times10^{-4}$ s^{-1}. Stress strain curve (red line) plotted with maximum temperature (black line) and AE cumulative energy (blue solid line – sensor VS900, blue dashed line – sensor VS45). Vertical dashed lines separate the stages I, II, and III

ing the early stages of deformation and in the non-linear stage below the yield point the temperature remains practically constant (apart from the slight oscillations around the nearly constant mean value). First with the deceleration of AE energy increment the maximum temperature starts to rise. There must be highlighted the unique cooperation/supplementation of AE and IRT techniques both of which seems to be sensitive to the different plastic deformation mechanisms. Maximum temperature shows basically the linear increase with progressing strain behind the yield point. This behaviour likely corresponds to the equality of heat dissipation with the heat generation at the strain rate of approx. $\dot{\varepsilon} = 7\times10^{-4}$ s^{-1}, which is still in a good agreement with the rate $\dot{\varepsilon} = 5\times10^{-4}$ s^{-1}, published for the same steel grade by Li et al. [7].

Representative results corresponding to the samples strained at the lower rate: $\dot{\varepsilon} = 1.4\times10^{-4}$ s^{-1}, are plotted on Fig. 2. Stress strain curve for strain rate ε· = 1.4×10–4 s–1. Stress strain curve (red line) plotted with maximum temperature (black line) and AE cumulative energy (blue solid line – sensor VS900, blue dashed line – sensor VS45). Vertical dashed lines separate the stages I, II, and III2.

Mechanical loading data show practically the same trend as in the case of faster straining, but the yield point is shifted to the higher strains and the non-linear region is even more prominent. AE cumulative energy increase follows the non-linear mechanical properties with only slight delay in the beginning of plastic deformation and some slight cumulation occurring even beyond the yield point. In addition to this area there is also the cumulation of hits in the quasi-linear part on the very beginning

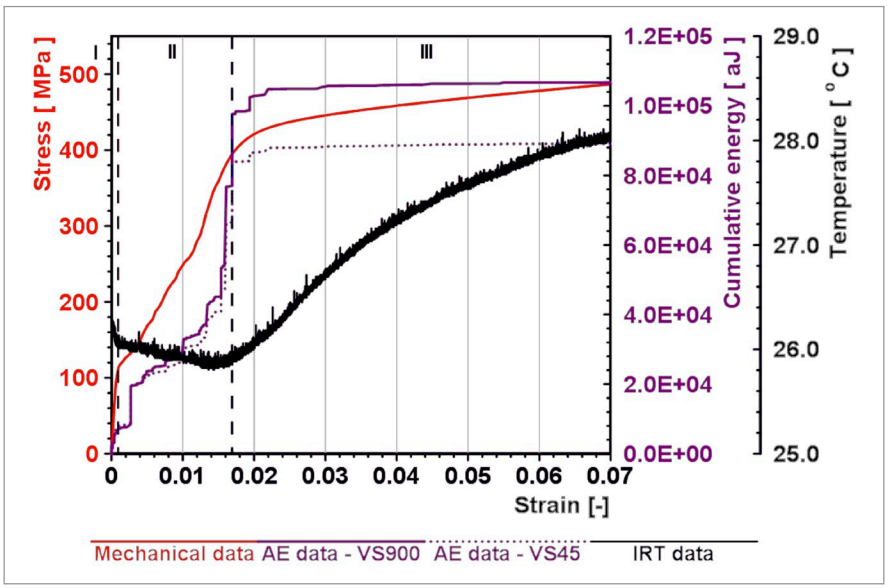

Fig. 2. Stress strain curve for strain rate $\dot{\varepsilon} = 1.4\times10^{-4}$ s^{-1}. Stress strain curve (red line) plotted with maximum temperature (black line) and AE cumulative energy (blue solid line – sensor VS900, blue dashed line – sensor VS45). Vertical dashed lines separate the stages I, II, and III

of deformation which was also the case in the faster loading. The overall amount of energy is however approximately one order of magnitude lower than in the following plastic bellow-yield stage. The character of maximum temperature at the lower strain rate appears differently. In the early stage of straining and in the below-yield-plastic deformation stage the maximum temperature first decreases. This effect was also reported by Kozlowska [12] as a characteristic of elastic deformation. In order to capture the temperature changes in the beginning of deformation, zoomed area below the strain 0.02 is visualized on Fig. 3. Zoomed onset of deformation of a sample strained at the rate ε· = 1.4×10–4 s–1. Vertical dashed lines separate the stages I, II, and III3.

It is interesting to point out, that the sharp decrease of maximum temperature in the very beginning of loading coincide very well with the quasi-linear deformation stage and is subsequently followed by gradual decrease during the below-yield plasticity. Sluggish cooling which is in a good agreement with the onset of non-linear stress-strain character thus most likely indicates the localized plastic deformation. With the progressing straining, maximum temperature monotonously rises having the concave character which is in contrary to the linear temperature rise at the rate $\dot{\varepsilon} = 7\times10^{-4}$ s^{-1}, Fig. 1. Stress strain curve for strain rate ε· = 7×10–4 s–1. Stress strain curve (red line) plotted with maximum temperature (black line) and AE cumulative energy (blue solid line – sensor VS900, blue dashed line – sensor VS45). Vertical dashed lines separate the stages I, II, and III1. Origin of this behaviour is probably the faster heat dissipation than the heat generation at the lower strain rate. The property of supplementing sensitivity of AE and IRT to different mechanisms is preserved even at the lower strain rate.

Analyses above strongly indicate that the loading under 7% could be sectioned into three principal stages where the consistent changes are prominent from all the three evaluated indicators: stress-strain curve, AE cumulative energy, ITR maximum temperature. Stage I in the very beginning of deformation is attributed to the prevailing elastic deformation. Some local plastic deformation on the stress concentrators could not be excluded which is the potential source of AE responses with low accumulated energy. These signals originate from the sample and not from a potential noise in the grips as the guard sensor technique excludes the hits with the first arrival on grips. Stage II corresponds to the plastic deformation bellow the assumed yield point which proceeds through the Shockley partial dislocations in austenite $\{111\}_\gamma$ planes, the stacking faults formed between partials respectively. With progressing deformation, the SFs may diverge and form the shear bands when exceeding some critical stress, proportional to the SFE of a material. Stage III thus most likely corresponds to the formation of shear bands as a result of overlapping of SFs in the $\{111\}_\gamma$ planes. If the regular overlapping occurs in every second $\{111\}_\gamma$ planes, transformation of ε-martensite takes place. Stage III could therefore be attributed to the formation of shear bands and transformation of ε-martensite.

4. Conclusions

Acoustic emission and infrared thermography have been deployed to study the low strain plastic deformation of AISI 304L SS. It was demonstrated that the combination of these two techniques is remarkably advantageous as both the cumulative AE energy and the maximum IRT temperature are supplementary in terms of the sensitivity to the different mechanisms. Three stages of deformation below 7% strain can be concluded with the following characteristics:

- Stage I is the elastic deformation. AE shows some activity with the low accumulated energy. IRT captures the relatively steep cooling of sample at the lower rate $\dot{\varepsilon} = 1.4\times10^{-4}$ s^{-1} and basically the constant temperature at faster straining $\dot{\varepsilon} = 7\times10^{-4}$ s^{-1}.

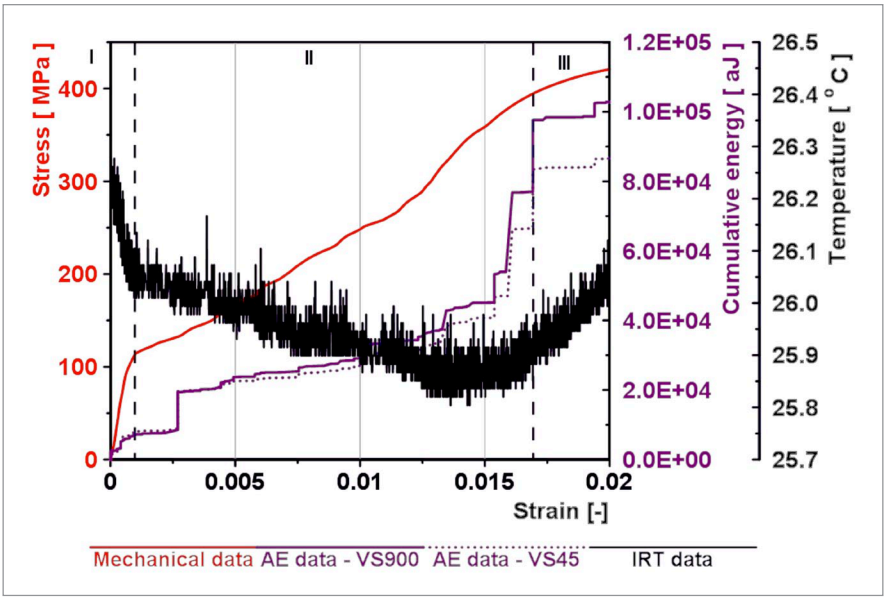

Fig. 3. Zoomed onset of deformation of a sample strained at the rate $\dot{\varepsilon} = 1.4\times10^{-4}$ s^{-1}. Vertical dashed lines separate the stages I, II, and III

- Stage II corresponds to the formation of Shockley partial dislocations and the SFs. AE displays the strong sensitivity to these mechanisms as the cumulative energy sharply rises, which is in the good coincidence with the area of strongly non-linear behaviour of stress strain curve. Cooling of the sample slows down at $\dot{\varepsilon} = 1.4\times10^{-4}$ s^{-1} as a result of the occurrence of plastic deformation in localized domains. The constant (slightly oscillating) trend is observed at the higher loading speed $\dot{\varepsilon} = 7\times10^{-4}$ s^{-1}.
- Stage III is attributed to the shear bands and ε-martensite formation. With respect to the previous stage AE starts to become quiet. On the other hand, the ITR supplements the AE output by sharp increase of maximum temperature. Strain rate $\dot{\varepsilon} = 7\times10^{-4}$ s^{-1} seems to be the speed where the heat generated equals the heat dissipated which is manifested by linear rise of maximum temperature with straining. The maximum temperature increase with strain shows rather concave characteristics at the lower rate $\dot{\varepsilon} = 1.4\times10^{-4}$ s^{-1}.

Acknowledgement

This work was financed by grant agency VEGA1/0510/20; KEGA 011ZU-4/2022. This publication is the result of support under the Operational Program Integrated Infrastructure for the project: Strategic implementation of additive technologies to strengthen the intervention capacities caused by the COVID-19 pandemic ITMS code: 313011ASY4, co-financed by the European Regional Development Fund. The work was also supported by the European Regional Development Fund in the Research Centre of Advanced Mechatronic Systems project, CZ.02.1.01/0.0/0.0/16_019/0000867 within the Operational Programme Research, Development and Education and the project SP2021/27 Advanced methods and technologies in the field of machine and process control supported by the Ministry of Education, Youth and Sports, Czech Republic. The support is acknowledged.

REFERENCES

[1] J.A. Rodríguez-Martínez, R. Pesci, A. Rusinek, Experimental study on the martensitic transformation in AISI 304 steel sheets subjected to tension under wide ranges of strain rate at room temperature, Materials Science and Engineering **A 528**, 5974-5982 (2011).

[2] K. Sato, M. Ichinose, Y. Hirotsu, Y. Inoue, Effects of Deformation Induced Phase Transformation and Twinning on the Mechanical Properties of Austenitic Fe-Mn-Al Alloys, ISIJ International **29**, 10, 868-877 (1989).

[3] S. Allain, J.-P. Chateau, O. Bouaziz, S. Migot, N. Guelton, Correlations between the calculated stacking fault energy and the plasticity mechanisms in Fe–Mn–C alloys, Materials Science and Engineering **A 387-389**, 158-162 (2004).

[4] E.I. Galindo-Nava, P.E.J. Rivera-Díaz-del-Castillo, Understanding martensite and twin formation in austenitic steels: A model describing TRIP and TWIP effects, Acta Materialia **128**, 120-134 (2017).

[5] R.E. Schramm, R.P. Reed, Stacking Fault Energies of Seven Commercial Austenitic Stainless Steels, Metallurgical Transactions A **6A**, 1345-1351 (1975).

[6] P.J. Brofman, G.S. Ansell, On the Effect of Carbon on the Stacking Fault Energy of Austenitic Stainless Steels, Metallurgical Transactions A **9**, 6, 879-880 (1978).

[7] X. Li, J. Chen, L. Ye, W. Ding, P. Song, Influence of Strain Rate on Tensile Characteristics of SUS304 Metastable Austenitic Stainless Steel, Acta Metallurgica Sinica **26**, 657-662 (2013).

[8] M. Šofer, P. Kučera, E. Mazancová, L. Krejčí, Acoustic Emission and Fractographic Analysis of Seamless Steel Pressure Cylinders with Artificial Flaws Under Hydrostatic Burst Testing, Journal of Nondestructive Evaluation **38**, 84 (2019).

[9] S.M.C. Van Bohemen, J. Sietsma, M.J.M. Hermans, I.M. Richardson, Analysis of acoustic emission signals originating from bainite and martensite formation, Philosophical Magazine **85**, 16, 1791-1804 (2005).

[10] J. Talonen, H. Hänninen, Formation of shear bands and strain-induced martensitu during plastic deformation of metastable austenitic stainless steels, Acta Materialia **55**, 6108-6118 (2007).

[11] N. Zreihan, E. Faran, E. Vives, A. Planes, D. Shilo, Relations between stress drops and acoustic emission measured during mechanical loading, Physical Review Materials (2019). DOI: https://doi.org/10.1103/PhysRevMaterials.3.043603

[12] B. Kozłowska, Application of thermography method to the investigation of two-dimensional elastic-plastic states, Archive of Mechanical Engineering **59**, 297-312 (2012).

[13] T.S. Byun, On the stress dependence of partial dislocation separation and deformation microstructure in austenitic stainless steels, Acta Materialia **51**, 3063-3071 (2003).

[14] Y.F. Shen, X.X. Li, X. Sun, Y.D. Wang, L. Zuo, Twinning and martensite in a 304 austenitic stainless stell, Materials Science and Engineering A **552**, 514-522 (2012).

[15] J. Liu, D. Kaoumi, Use of in-situ TEM to characterize the deformation-induced martensitic transformation in 304 stainless steel at cryogenic temperature, Materials Characterization, pp. 331-336 (2018).

[16] N. Li, Y.D. Wang, W.J. Liu, Z.N. An, J.P. Liu, R. Su, J. Li, P.K. Liaw, In situ X-ray microdiffraction study of deformation-induced phase transformation in 304 austenitic stainless steel, Acta Materialia **64**, 12-23 (2014).

[17] D. Kaoumi, J. Liu, Deformation induced martensitic transformation in 304 austenitic stainless steel: In-situ vs. ex-situ transmission electron microscopy characterization, Material Science & Engineering, pp. 73-82 (2018).

[18] T.F.A. Santos, M.S. Andrade, Avaliação dilatométrica da reversão das martensitas induzidas por deformação em um aço inoxidável austenítico do tipo ABNT 304, Matéria (Rio de Janeiro) **13** (4), 587-596 (2008).

[19] G. Cios, T. Tokarski, A. Zywczak, R. Dziurka, M. Stepien, L. Gondek, M. Marciszko, B. Pawiowski, K. Wieczerzak, P. Baia, The Investigation of Strain-Induced Martensite Reverse Transformation in AISI 304 Austenitic Stainless Steel, Metallurgical And Materials Transactions A **48A**, 4999-5008 (2017).

[20] E.V. Legostaeva, Yu.P. Sharkeev, A.Yu. Eroshenko, O.A. Belyavskaya, V.P. Vavilov, V.A. Skrypnyak, A.M. Ustinov, A.A. Klopotov, A.O. Chulkov, A.A. Kozulin, P.V. Uvarkin, V.V. Skrypnyak, Influence of Zr-1 wt.% Nb alloy structure state on its deformation and thermal behavior under quasi-static tension, Materiala Latters **285** (2021). DOI: https://doi.org/10.1016/j.matlet.2020.129028

[21] G.C. Soares, Y.P. Sharkeev, A.Y. Eroshenko, A.A.A.Y. Belyavskaya, V.P. Vavilov, V.A. Skrypnyak, A.M. Ustinov, A.A. Klopotov, A.O. Chulkov, A.A. Kozulin, Thermomechanical Behaviour of Steels in Tension Studied with Synchronized Full-Field Deformation and Temperature Measurements, Experimental Techniques (2021). DOI: https://doi.org/10.1007/s40799-020-00436-y

[22] Z. Vesely, M. Honner, Infrared Camera Comparative Measurement Methods for Thermally Optical Properties of Materials, AIP Conference Proceedings **2133** (2019).
DOI: https://doi.org/10.1063/1.5120170

[23] P. Honnerová, J. Martan, Z. Veselý, M. Honner, Method for emissivity measurement of semitransparent coatings at ambient temperature, Scientific Reports **7** (2017).
DOI: https://doi.org/10.1038/s41598-017-01574-x